DALTON

Syntheses and characterisation of mono- and di-nuclear iron(III) complexes of 1,4,7-triazacyclononane-*N*-acetate (L). Crystal structures of $[FeCl_2L]$ and $[Fe_2(\mu\text{-}O)(\mu\text{-}O_2CMe)L_2]ClO_4\cdot NaClO_4\cdot 2H_2O$†

Bim Graham,[a] Boujemaa Moubaraki,[a] Keith S. Murray,[a] Leone Spiccia,*[,a] John D. Cashion[b] and David C. R. Hockless[c]

[a] *Department of Chemistry, Monash University, Clayton, Victoria, 3168, Australia*
[b] *Department of Physics, Monash University, Clayton, Victoria, 3168, Australia*
[c] *Research School of Chemistry, Australian National University, Canberra, ACT, 0200, Australia*

The macrocycle 1,4,7-triazacyclononane-*N*-acetate (L) reacted with $FeCl_3\cdot 6H_2O$ in water to form the monomeric complex $[FeCl_2L]$ **1**. Hydrolysis of **1** in the presence of an excess of sodium acetate and sodium perchlorate yielded the binuclear complex $[Fe_2(\mu\text{-}O)(\mu\text{-}O_2CMe)L_2]ClO_4\cdot NaClO_4\cdot 2H_2O$ **2**. Complexes **1** and **2** have been characterised by X-ray crystallography. In **1** the Fe^{III} is surrounded by a distorted-octahedral array of one *fac*-co-ordinated triamine ring, one monodentate carboxylato group and two chloride ligands. Complex **2** consists of a μ-oxo-μ-acetato-diiron(III) core with the distorted octahedral co-ordination sphere about each Fe^{III} being completed by the ligand L. A sodium ion, with distorted trigonal-bipyramidal stereochemistry, bridges between the co-ordinating carboxylate oxygens of the terminal ligands. Complex **2** exhibits spectroscopic features and magnetic properties similar to those of other μ-oxo-diiron(III) complexes as well as metalloproteins incorporating a μ-oxo-diiron(III) unit at their active sites.

Complexes possessing μ-oxo- or μ-hydroxo-diiron cores continue to contribute to the understanding of specific types of non-haem, non-sulfur iron proteins containing these structural motifs at their active sites.[1] Such proteins perform a variety of functions, such as dioxygen transport and storage (haemerythrin),[2] conversion of ribonucleotides into deoxyribonucleotides in DNA synthesis (ribonucleotide reductase),[3] alkane hydroxylation (methane monooxygenase)[4] and phosphate ester hydrolysis (purple acid phosphatase).[5] Within these metalloproteins considerable variation exists both in the number and types of terminal ligands which cap the μ-oxo- or μ-hydroxo-diiron unit and in the ligands which bridge the iron centres in addition to the oxo/hydroxo group. Modelling studies have sought to elucidate how these structural variations influence the intrinsic spectral and magnetic properties of the μ-oxo- or μ-hydroxo-diiron unit and tune the sites for their specific biological functions.

The first oxo-bridged complexes prepared consist of triply-bridged μ-oxo-bis(μ-carboxylato)diiron structural units capped by tridentate, facially co-ordinating ligands such as 1,4,7-triazacyclononane,[6] *N*,*N*′,*N*″-trimethyl-1,4,7-triazacyclononane[7] and hydrotris(pyrazol-1-yl)borate.[8] These synthetic analogues mimic remarkably well the spectroscopic[2b] and magnetic properties[9] of the met-azido form of haemerythrin, which contains a μ-oxo-bis(μ-carboxylato)diiron core terminally co-ordinated by five histidine residues and an exogenous N_3^- ligand (Fig. 1).[10] More recently, Que and co-workers[11] have reported a series of doubly bridged μ-oxo-μ-carboxylato-diiron(III) complexes in which the co-ordination sphere of each iron is completed by a tetradentate tripodal ligand. These complexes more closely duplicate the μ-oxo-μ-carboxylato-diiron(III) unit found in the B2 subunit of ribonucleotide reductase from *Escherichia coli* (Fig. 1).[12] Carboxylate groups have been incorporated into a number of tetradentate ligands in order to approach the oxygen-rich co-ordination environment found in this protein.[11c]

† *Non-SI unit employed:* $\mu_B \approx 9.27 \times 10^{-24}$ J T^{-1}.

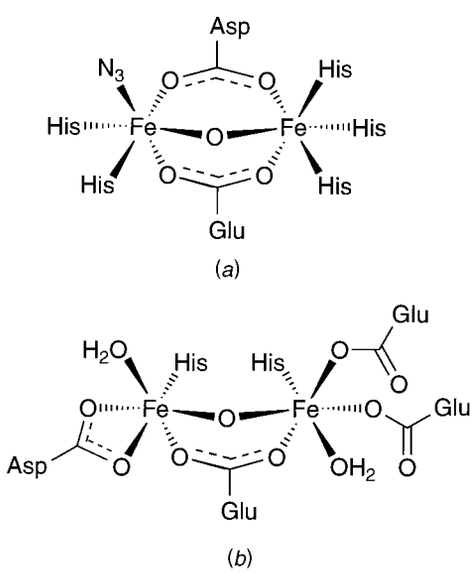

Fig. 1 Active sites of (*a*) met-azidohaemerythrin and (*b*) the B2 subunit of ribonucleotide reductase

We were interested in stabilising an oxo-bridged diiron(III) core by using the tetradentate pendant arm-bearing macrocycle 1,4,7-triazacyclononane-*N*-acetate (L). It was anticipated that L would promote the formation of a μ-oxo-μ-carboxylato-diiron(III) complex incorporating terminally co-ordinating carboxylate groups, thus producing a model for the active site of ribonucleotide reductase B2. We report herein the complexation of L with Fe^{III} to form $[FeCl_2L]$ and the generation of the oxo-bridged diiron(III) complex $[Fe_2(\mu\text{-}O)(\mu\text{-}O_2CMe)L_2]ClO_4\cdot NaClO_4\cdot 2H_2O$ by hydrolysis of this monomeric species. The crystal structures and physicochemical properties of both complexes are presented and those of the dinuclear complex discussed with reference to other complexes incorporating the μ-oxo-diiron(III) unit.

Table 1 Selected bond lengths (Å) and angles (°) for complex **1**

Fe–Cl(1)	2.282(2)	Fe–Cl(2)	2.346(2)
Fe–O(1)	1.955(4)	Fe–N(1)	2.227(5)
Fe–N(2)	2.185(6)	Fe–N(3)	2.144(6)
O(1)–C(8)	1.289(8)	O(2)–C(8)	1.221(8)
Cl(1)–Fe–Cl(2)	97.22(7)	Cl(1)–Fe–O(1)	99.1(1)
Cl(1)–Fe–N(1)	169.9(1)	Cl(1)–Fe–N(2)	92.7(1)
Cl(1)–Fe–N(3)	102.8(2)	Cl(2)–Fe–O(1)	95.4(1)
Cl(2)–Fe–N(1)	92.7(1)	Cl(2)–Fe–N(2)	166.0(2)
Cl(2)–Fe–N(3)	89.5(2)	O(1)–Fe–N(1)	78.0(2)
O(1)–Fe–N(2)	92.7(2)	O(1)–Fe–N(3)	156.8(2)
N(1)–Fe–N(2)	77.9(2)	N(1)–Fe–N(3)	79.2(2)
N(2)–Fe–N(3)	78.7(2)	Fe–O(1)–C(8)	119.7(4)

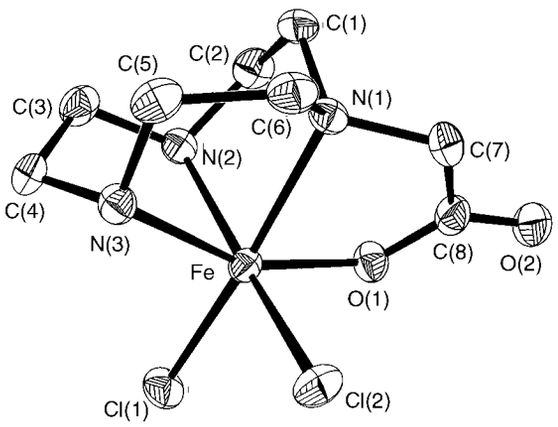

Fig. 2 An ORTEP[16] plot of complex **1** with the atomic labelling scheme

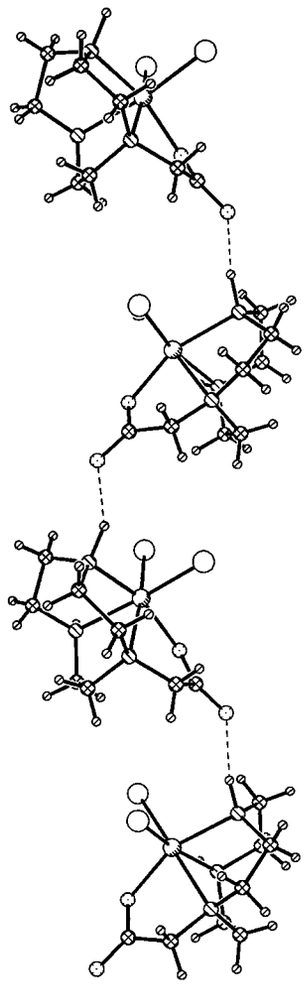

Fig. 3 Packing scheme for complex **1** showing hydrogen-bond contacts

Results and Discussion

$[FeCl_2L]$ 1

Addition of $FeCl_3·6H_2O$ to an aqueous solution of L,[13,14] pre-adjusted to pH 7, led to a rapid decrease in pH to approximately 2. Since the ligand is partially protonated at pH 7 this observation is indicative of complex formation. Orange-yellow crystals of $[FeCl_2L]$ **1** precipitated on standing and proved suitable for X-ray structure determination. Electron microprobe and elemental analysis confirmed the composition of the complex. In the IR spectrum bands at 3272 and 3204 cm^{-1} are attributed to N–H stretches of the secondary amines in the ligand. The presence of two such bands is indicative of two N–H environments. This was confirmed by the crystal structure, which shows that one secondary amine is involved in hydrogen bonding (see below). Strong bands at 1660 and 1325 cm^{-1} are due to the asymmetric and symmetric stretching modes of the carboxylate group, the large separation between them being indicative of monodentate co-ordination.[15]

Details of the crystal structure solution and refinement for complex **1** are given in the Experimental section and Table 5, selected bond lengths and angles are presented in Table 1 and a view of the neutral complex is shown in Fig. 2. The complex is monomeric with the Fe^{III} co-ordinated facially by the macrocyclic ring of L; the carboxylate pendant arm, binding in a monodentate fashion, and two *cis*-oriented chloride ligands complete the distorted-octahedral co-ordination sphere. The tetradentate co-ordination mode of L leads to the formation of one FeNCCO and three FeNCCN five-membered chelate rings, each of which is puckered. The three N_{cis}–Fe–N_{cis} angles are all well below the 90° expected for an idealised octahedral structure, averaging 78.6(6)°, owing to the inflexibility of the macrocycle in forming three fused five-membered chelate rings. The N(1)–Fe–O(1) angle is also significantly reduced below 90° due to the N(1) and O(1) atoms forming part of the same five-membered chelate ring. The two Fe–Cl bonds are inequivalent, with Fe–Cl(1) bond shortened 0.064(4) Å relative to the Fe–Cl(2). This may be traced to the reduced electron-donating power of the tertiary nitrogen N(1) [*trans* to Cl(1)] relative to the secondary nitrogen N(2) [*trans* to Cl(2)], as indicated by the somewhat lengthened Fe–N(1) bond compared to the Fe–N(2) [2.227(5) *versus* 2.185(6) Å]. The Fe–N bonds *trans* to the chloride ligands [average 2.206(6) Å] are lengthened slightly relative to Fe–N(3) *trans* to the carboxylate group [2.144(6) Å], possibly because of the greater *trans* influence of the chloro groups.

Within the lattice of complex **1** the N(3)H hydrogen atom of each complex unit forms a strong hydrogen-bond contact to the carboxylate O(2) atom of a neighbouring complex unit (symmetry operation: x, $2 - y$, $\frac{1}{2} + z$) of 2.00 Å [N(3)···O(2) 2.846(7) Å]. This leads to one-dimensional chains of hydrogen bonds extending throughout the lattice running parallel to the *c* axis (Fig. 3).

$[Fe_2(\mu\text{-}O)(\mu\text{-}O_2CMe)L_2]ClO_4·NaClO_4·2H_2O$ 2

Hydrolysis of complex **1** in aqueous sodium acetate solution and addition of sodium perchlorate produced a brownish green solution. Slow evaporation of this mixture yielded dark green crystals of $[Fe_2(\mu\text{-}O)(\mu\text{-}O_2CMe)L_2]ClO_4·NaClO_4·2H_2O$ **2** suitable for single-crystal X-ray crystallography. Electron microprobe analysis confirmed the presence of Fe, Na and Cl, while elemental analysis was consistent with the given formula. In the IR spectrum an O–H stretch at 3622 cm^{-1} confirmed the presence of water of crystallisation, an N–H stretch at 3312 cm^{-1} the presence of the amino groups of the ligand, and the bands

Table 2 Selected bond lengths (Å) and angles (°) for complex **2**

Fe(1)–O(1)	2.000(6)	Fe(1)–O(3)	1.786(5)
Fe(1)–O(4)	2.016(5)	Fe(1)–N(1)	2.242(6)
Fe(1)–N(2)	2.161(7)	Fe(1)–N(3)	2.155(7)
Fe(2)–O(3)	1.793(5)	Fe(2)–O(5)	2.030(5)
Fe(2)–O(6)	2.010(6)	Fe(2)–N(4)	2.249(7)
Fe(2)–N(5)	2.173(6)	Fe(2)–N(6)	2.164(7)
Na–O(1)	2.340(7)	Na–O(01)	2.315(7)
Na–O(02)	2.285(7)	Na–O(6)	2.524(6)
Na–O(1)	2.359(8)	O(1)–C(8)	1.295(9)
O(2)–C(8)	1.230(9)	O(4)–C(9)	1.274(9)
O(5)–C(9)	1.258(9)	O(6)–C(18)	1.32(1)
O(7)–C(18)	1.20(1)		
O(1)–Fe(1)–O(3)	101.2(2)	O(1)–Fe(1)–O(4)	91.1(2)
O(1)–Fe(1)–N(1)	77.9(2)	O(1)–Fe(1)–N(2)	94.3(2)
O(1)–Fe(1)–N(3)	156.2(2)	O(3)–Fe(1)–O(4)	100.6(2)
O(3)–Fe(1)–N(1)	172.8(2)	O(3)–Fe(1)–N(2)	94.9(2)
O(3)–Fe(1)–N(3)	102.2(3)	O(4)–Fe(1)–N(1)	86.6(2)
O(4)–Fe(1)–N(2)	162.3(2)	O(4)–Fe(1)–N(3)	88.7(3)
N(1)–Fe(1)–N(2)	78.0(3)	N(1)–Fe(1)–N(3)	78.3(3)
N(2)–Fe(1)–N(3)	79.6(3)	O(3)–Fe(2)–O(5)	100.5(2)
O(3)–Fe(2)–O(6)	103.4(2)	O(3)–Fe(2)–N(4)	172.2(2)
O(3)–Fe(2)–N(5)	94.1(2)	O(3)–Fe(2)–N(6)	99.8(3)
O(5)–Fe(2)–O(6)	92.0(3)	O(5)–Fe(2)–N(4)	86.9(2)
O(5)–Fe(2)–N(5)	162.2(2)	O(5)–Fe(2)–N(6)	88.5(3)
O(6)–Fe(2)–N(4)	78.7(2)	O(6)–Fe(2)–N(5)	94.5(3)
O(6)–Fe(2)–N(6)	156.4(3)	N(4)–Fe(2)–N(5)	78.2(2)
N(4)–Fe(2)–N(6)	77.8(2)	N(5)–Fe(2)–N(6)	78.9(3)
O(1)–Na–O(01)	89.3(2)	O(1)–Na–O(02)	148.6(3)
O(1)–Na–O(6)	91.6(2)	O(1)–Na–O(11)	110.4(3)
O(01)–Na–O(02)	95.3(3)	O(01)–Na–O(6)	178.3(3)
O(01)–Na–O(11)	97.7(3)	O(02)–Na–O(6)	83.2(2)
O(02)–Na–O(11)	99.8(3)	O(6)–Na–O(11)	83.4(2)
Fe(1)–O(1)–Na	121.8(2)	Fe(1)–O(1)–C(8)	118.1(5)
Na–O(1)–C(8)	118.8(5)	Fe(1)–O(3)–Fe(2)	127.7(3)
Fe(1)–O(4)–C(9)	132.0(5)	Fe(2)–O(5)–C(9)	130.7(5)
Fe(2)–O(6)–Na	116.3(3)	Fe(2)–O(6)–C(18)	118.5(5)
Na–O(6)–C(18)	125.2(6)		

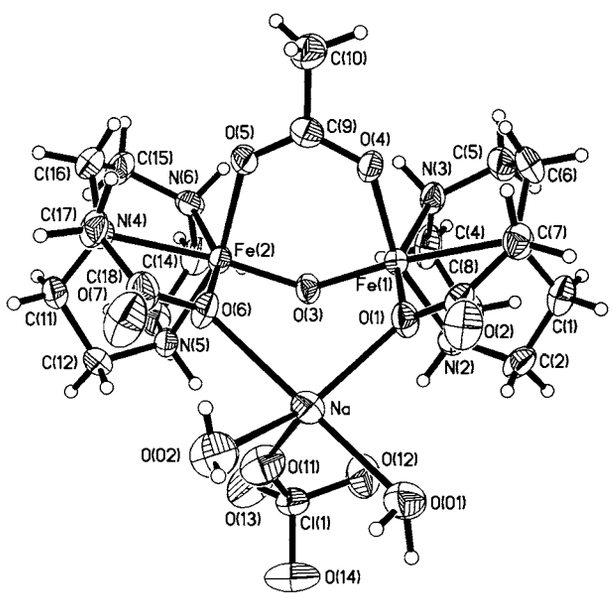

Fig. 4 An ORTEP[16] plot of the diiron(III) unit of complex **2** with the atomic labelling scheme

at 1092 and 625 cm^{-1} the presence of perchlorate counter ions. The presence of the bridging acetate in the complex is indicated by bands at 1543 and 1450 cm^{-1}, while bands at 1636, 1347 and 1308 cm^{-1} are due to the monodentate pendant carboxyl groups of the ligand.

Details of the crystal structure solution and refinement for complex **2** are given in the Experimental section and Table 5, selected bond lengths and angles in Table 2 and a view of the complex is shown in Fig. 4. Table 3 compares the salient structural features of **2** with those of a range of other μ-oxo-diiron(III) complexes and the active sites of met-azidohaemerythrin and ribonucleotide reductase B2. The structure of **2** consists of a doubly bridged μ-oxo-μ-acetato-diiron(III) unit with the distorted-octahedral co-ordination sphere about each of the two Fe^{III} being completed by the tetradentate ligand L. As in **1**, the deviation from idealised octahedral geometry is due largely to the requirements of L in forming four edge-sharing, five-membered chelate rings, leading to acute N_{cis}–Fe–N_{cis} and N–Fe–$O_{pendant}$ bite angles. The single acetate bridge restricts the Fe(1)–O(3)–Fe(2) angle to 127.7(3)° and the Fe(1)···Fe(2) distance to 3.2128(1) Å. These values are typical of those found for other μ-oxo-μ-carboxylato-diiron(III) complexes, which typically show Fe–O–Fe angles of 129 ± 1° and Fe···Fe separations of 3.21 ± 0.01 Å,[11] but are slightly larger than the corresponding values of 120 ± 5° and 3.12 ± 0.05 Å observed for triply bridged μ-oxo-bis(μ-carboxylato)diiron(III) species.[1d,g] Interestingly, the dimensions of the μ-oxo-diiron(III) core for **2** (and doubly bridged complexes in general) more closely approach those found for the diiron(III) sites in met-azidohaemerythrin[10] and ribonucleotide reductase B2[12,17] than do those of most triply bridged species. The Fe–N bonds *trans* to the oxo bridge in **2** [average 2.27(1) Å] are significantly lengthened relative to those *trans* to the acetato bridge or terminal carboxylates [average 2.16(3) Å] due to the greater *trans* influence of the oxo bridge. The latter gives rise to short Fe–O(3) bonds [average 1.790(5) Å], typical of those found for other μ-oxo-diiron(III) complexes.[1g,20]

The acetate pendant arm oxygens, O(1) and O(6), which co-ordinate to the Fe^{III} are also involved in bonding interactions with the sodium cation present in complex **2**. The Na–O(1) and Na–O(6) distances differ significantly [2.340(7) *versus* 2.524(6) Å], however both fall into the normal range for Na···O bond contacts.[21] The inequivalent interaction of the sodium ion with the two halves of the dinuclear unit introduces a slight asymmetry into the complex, since the two halves would otherwise be related by a mirror plane bisecting the Fe(1)–O(3)–Fe(2) unit, Bridging O···Na^+···O interactions have previously been observed in the solid-state structures of complexes such as Na[Cu(tcta)]·2NaBr·8H_2O (tcta = 1,4,7-triazacyclononane-*N*,*N*′,*N*″-triacetate)[22] and [Co(salen)Na(thf)$_4$] [H_2salen = 1,2-bis(salicylidene)ethane-1,2-diamine, thf = tetrahydrofuran].[23] Lithium ion–carboxylate contacts also exist in the copper(II) complex of L, [CuClL]·LiCl·2H_2O, although in this case bonding to the lithium cation occurs through the carbonyl oxygen of the carboxylate pendant of L.[24] The geometry about the sodium ion in **2** is distorted trigonal bipyramidal, with the sodium being bound by two water molecules, H_2O(01) and H_2O(02), and the oxygen atom, O(11), of a perchlorate anion, in addition to O(1) and O(6). Although octahedral stereochemistry is most common for sodium ions, this stereochemistry has been observed previously.[21] The sodium-bound water molecule, H_2O(02), forms a hydrogen-bond contact to the carbonyl oxygen atom, O(7), of one of the acetate pendant arms, whilst H_2O(01) is hydrogen bonded to the carbonyl oxygen, O(2), of a neighbouring complex unit (symmetry operation: $x - \frac{1}{2}, 1 - y, z$).

Physical properties of the iron(III) complexes

Fig. 5 shows the temperature dependence of the effective magnetic moments, per Fe^{III}, of complexes **1** and **2**. The magnetic moment of **1** shows only a very gradual decrease over the temperature range 300–100 K, with a value of 5.66 μ_B at 300 K similar to that found for mononuclear high-spin d^5 iron(III) complexes. Below 100 K the magnetic moment begins to decrease more dramatically, reaching a value of 3.50 μ_B at 4.5 K, indicating the presence of weak antiferromagnetic coupling. This interaction is thought to be mediated through the parallel

Table 3 Comparison of X-ray structural, magnetic and Mössbauer parameters for complex **2** and selected μ-oxo-diiron(III) complexes and proteins

Complex	Fe···Fe/Å	Fe–oxo[a]/Å	Fe–O–Fe/°	$-J$/cm^{-1}	g	δ/mm s^{-1}	ΔE_Q/mm s^{-1}
2	3.2128(1)	1.790(5)	127.7(3)	109	1.99	0.45	1.58
$[Fe_2O(O_2CMe)(tpma)_2]^{3+}$ [b]	3.243(1)	1.795(5)	129.2(2)	114	2.03	0.45	1.45
$[Fe_2O(O_2CPh)(bpmg)_2]^{+}$ [c]	3.223(6)	1.782(6)	129.8(3)	120	2.00	*d*	*d*
$[Fe_2O(O_2CMe)_2(tacn)_2]^{2+}$ [e]	3.063(2)	1.781(4)	118.7(4)	*d*	*d*	0.46	1.72
$[Fe_2O(O_2CMe)_2(tmtacn)_2]^{2+}$ [f]	3.12(1)	1.800(3)	119.7(1)	115	*g*	0.47	1.50
met-Azidohaemerythrin[h]	3.25	1.77	135	134[i]	2.00	0.51, 0.51	1.47, 1.95
Ribonucleotide reductase B2[j]	3.3 (3.22)[k,l]	(1.78)[t]	(130)[l,m]	108	*g*	0.53, 0.44	1.66, 2.45

[a] Average. [b] tpma = Tris(2-pyridylmethyl)amine; ref. 11(*a*) and 11(*b*). [c] Hbpmg = *N*,*N*-Bis(2-pyridylmethyl)glycine; ref. 11(*c*). [d] Not measured. [e] tacn = 1,4,7-Triazacyclononane; ref. 6. [f] tmtacn = *N*,*N*′,*N*″-Trimethyl-1,4,7-triazacyclononane; ref. 7. [g] Not reported. [h] Refs. 10 and 18. [i] Measured for met-haemerythrin; ref. 9. [j] Refs. 3(*d*), 12, 17(*a*) and 19. [k] Extended X-ray absorption fine structure data in parentheses. [l] Not reported for crystal structure. [m] Calculated assuming iron–oxo distances are equal.

Table 4 Comparison of electronic spectroscopic data for selected μ-oxo-diiron(III) complexes and proteins

	λ_{max}/nm (ε/10^3 dm^3 mol^{-1} cm^{-1} per Fe_2)[a]			
Complex	$O^{2-}\rightarrow$Fe c.t.[b]	$^6A_1 \longrightarrow (^4T_2)(^4D)$, $^6A_1 \longrightarrow (^4E, {}^4A_1)(^4G)$, $O^{2-}\rightarrow$Fe c.t.[c]	$^6A_1 \longrightarrow {}^4T_2$, $O^{2-}\rightarrow$Fe c.t.[d]	$^6A_1 \longrightarrow {}^4T_1$[d]
$[Fe_2O(O_2CMe)(tpma)_2]^{3+}$ [e]	332 (10), 366 (sh)	460 (1.2), 429 (1.0), 504 (0.98), 534 (sh)	700 (0.16)	1950 (0.009)
2	323 (12.6), 360 (sh)	419 (1.5), 441 (1.3), 488 (sh), 498 (0.82), 527 (sh)	660 (0.15)	970 (0.007)
$[Fe_2O(O_2CPh)(bpmg)_2]^{+}$ [e]	320 (10), 355 (sh)	414 (1.1), 470 (sh), 488 (0.7), 520 (sh)	636 (0.16)	920 (0.007)
$[Fe_2O(O_2CMe)(cpmg)_2]^{-}$ [f]	310 (6.0)	402 (0.9, sh), 476 (0.25), 510 (0.15)	585 (0.11)	*g*
$[Fe_2O(O_2CMe)_2(tacn)_2]^{2+}$ [h]	333 (7.4), 368 (sh)	420 (sh), 468 (1.3), 492 (sh), 508 (sh), 544 (sh)	745 (0.14)	*g*
$[Fe_2O(O_2CMe)_2(tmtacn)_2]^{2+}$ [i]	345 (10.5)	424 (0.96), 472 (1.4), 513 (1.1), 549 (sh)	729 (0.14)	1031 (0.007)
met-Azidohaemerythrin[j]	326 (6.8), 380 (sh)	446 (3.7, br)	680 (0.19)	1010 (0.010)
Ribonucleotide reductase B2[k]	325 (9.4), 370 (7.2)	500 (0.8, br)	600 (0.30)	*g*

[a] Complex spectra recorded in MeCN unless indicated otherwise. [b] Ref. 27(*a*). [c] Ref. 27(*a*) and (*c*)–(*e*). [d] Refs. 6(*b*) and 27. [e] Ref. 11(*c*). [f] H_2cpmg = *N*-Carboxymethyl-*N*-(2-pyridylmethyl)glycine; ref. 11(*c*). [g] Not reported. [h] Ref. 6(*b*). [i] Ref. 7(*b*); recorded in MeOH. [j] Ref. 2(*b*). [k] Ref. 3(*d*).

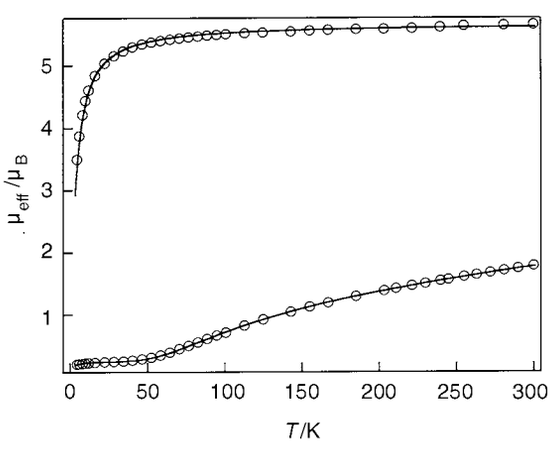

Fig. 5 Temperature dependence of the magnetic moment μ_{eff}, per Fe^{III}, for complex **1** (top) and **2** (bottom). The solid lines correspond to the theoretical fits to the data (dots)

one-dimensional chains of hydrogen bonds extending throughout the lattice of **1** (see above) and has been successfully fitted by a Fischer chain model ($S = \frac{5}{2}$) with $J = -0.31$ cm^{-1} and $g = 1.92$. Very weak intermolecular antiferromagnetic exchange coupling, arising from N–H···O_2CR interactions, has also been observed for two of the copper complexes of L reported by Wieghardt and co-workers.[24]

The data for complex **2** indicate strong antiferromagnetic coupling between the iron(III) centres, with the magnetic moment, per Fe^{III}, decreasing from 1.78 μ_B at 300 K to 0.21 μ_B at 4.5 K, and have been fitted well by a model of an isolated Heisenberg dimer of $S = \frac{5}{2}$ ions with the Hamiltonian $H = -2JS_1S_2$. The J value (−109 cm^{-1}) obtained implies stronger coupling than that usually observed for singly bridged μ-oxo-diiron(III) compounds, which exhibit J values of −80 to −105 cm^{-1},[20] but is slightly smaller than that typically found for μ-oxo-μ-carboxylato- and μ-oxo-bis(μ-carboxylato)-diiron(III) complexes,[1g] examples of which are listed in Table 3. Murray[20] and Que and co-workers[11a] have previously noted that the strength of antiferromagnetic coupling appears to be chiefly a property of the Fe–O–Fe unit and is largely insensitive to the nature of the terminal ligands which cap the unit or the number of carboxylates which bridge the iron(III) centres. Gorun and Lippard[25] have correlated the strength of antiferromagnetic coupling in multiply bridged diiron(III) centres incorporating a ligand oxygen atom bridge with the parameter P, defined as half the distance of the shortest superexchange pathway between the iron centres, according to the relation $-J = A\exp(BP)$, with $A = 8.763 \times 10^{11}$ and $B = -12.663$. For **2**, P is the average length of the iron–oxo bonds, since the shortest exchange route between the iron(III) centres occurs *via* the oxo-bridge. The calculated J value of −125 cm^{-1} compares reasonably well with that determined experimentally.

The Mössbauer spectrum of complex **1** recorded at 77 K shows a single sharp quadrupole doublet with isomer shift $\delta = 0.42$ mm s^{-1} and quadrupole splitting $\Delta E_Q = 0.59$ mm s^{-1}. These values lie within the ranges found for mononuclear high-spin iron(III) systems.[26] The Mössbauer spectrum of **2** consists of a single symmetrical quadrupole doublet with an isomer shift ($\delta = 0.45$ mm s^{-1}) characteristic, again, of a high-spin iron(III) centre, and a large quadrupole splitting ($\Delta E_Q = 1.58$ mm s^{-1}) due to the presence of six-co-ordinate Fe^{III} in an oxo-bridged dimer.[1d,g,20] These parameters are comparable to those found for other μ-oxo-diiron(III) complexes (Table 3). The presence of only one quadrupole-split absorption, however, indicates that **2**, despite the slight asymmetry introduced by the presence of the sodium ion, fails to model the asymmetry of the diiron(III) sites of met-azidohaemerythrin and ribonucleotide reductase B2. The Mössbauer data for these proteins show two distinct quadrupole-split pairs of absorptions, consistent with the presence of two inequivalent iron sites.[18,19] The absorption parameters for **2** are similar to those of one of the absorptions in the spectra of the proteins.

The electronic spectrum of complex **2** recorded in acetonitrile

Table 5 Crystallographic data for complexes **1** and **2**

	1	**2**
Formula	$C_8H_{16}Cl_2FeN_3O_2$	$C_{18}H_{39}Cl_2Fe_2N_6NaO_{17}$
M	312.99	817.13
Crystal system	Monoclinic	Orthorhombic
Space group	*Cc* (no. 9)	$Pca2_1$ (no. 29)
a/Å	12.6445(7)	10.590(2)
b/Å	7.2495(8)	19.509(2)
c/Å	14.0940(9)	15.670(2)
β/°	110.723(4)	
U/Å^3	1208.4(2)	3237.3(7)
Z	4	4
D_c/g cm^{-3}	1.720	1.676
λ/Å	1.541 78 (Cu-Kα)	0.710 69 (Mo-Kα)
F(000)	644	1688
μ/cm^{-1}	140.17	11.54
Transmission factor range	0.6447–1.0000	0.9492–1.000
$2\theta_{max}$/°; data collected	120.1; ±*h*, +*k*, −*l*	50.1; +*h*, −*k*, −*l*
No. data measured	1026	3258
No. unique data	983	3258
No. observed data [$I \geqslant 3.0\sigma(I)$]	858	2138
No. parameters refined	144	414
R^a	0.025	0.036
R'^b	0.026	0.033
Goodness of fit	2.67	1.94
Maximum Δ/σ	<0.01	<0.01
Maximum Δρ/e Å^{-3}	0.37	0.35

^{a} $R(F) = \Sigma(|F_o| - |F_c|)$. ^{b} $R' = [\Sigma w(|F_o| - |F_c|)^2/\Sigma wF_o^2]^{\frac{1}{2}}$, $w = [\sigma^2(F_o)]^{-1}$.

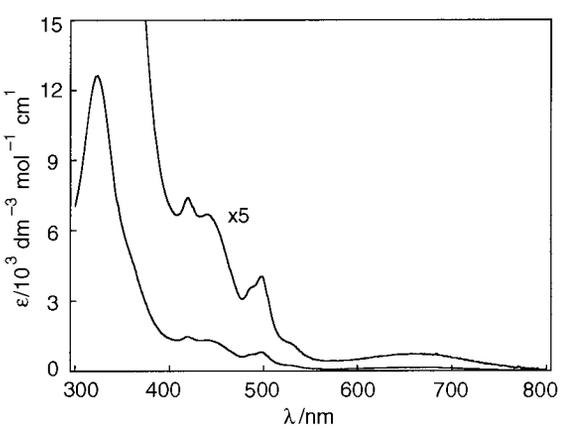

Fig. 6 Electronic spectrum of complex **2** in acetonitrile

is shown in Fig. 6. Table 4 compares the spectroscopic data with those of other μ-oxo-diiron(III) complexes and proteins and gives the currently accepted band assignments.[6b,27] The near-IR band in the 900–1000 nm region is attributed to a $^6A_1 \longrightarrow {}^4T_1$ transition, while that in the region 600–800 nm is believed to be primarily due to a forbidden $O^{2-} \rightarrow Fe$ charge-transfer (c.t.) transition which obscures a weaker $^6A_1 \longrightarrow {}^4T_2$ ligand-field transition. Both ligand-field transitions (some of which are forbidden) and a forbidden $O^{2-} \rightarrow Fe$ c.t. transition contribute to the complicated features in the 400–600 nm region. The intense band at 323 nm is due to an allowed $O^{2-} \rightarrow Fe$ c.t. transition. Mènage and Que[11c] noted that a general blue shift occurs in a number of the bands as aliphatic amines are replaced by aromatic amines and then carboxylate groups in the terminal ligands. The blue shift in ligand-field transitions is attributed to replacement of strong-field by weaker-field ligands, whilst for the $O^{2-} \rightarrow Fe$ c.t. transitions the trend is rationalised in terms of increasing neutralisation of the Lewis acidity of the iron(III) centres; aliphatic amines interact more weakly with iron centres than do aromatic amines, which in turn interact more weakly than do negatively charged carboxylate ligands. Complex **2** fits well into the series of doubly bridged μ-oxo-μ-carboxylato-diiron(III) complexes incorporating the neutral tetradentate ligand tpma, singly charged cpmg and doubly charged cpmg, with bands lying intermediate between those of the tmpa and bpmg complexes.

The spectroscopic features observed for complex **2** are very similar to those exhibited by the diiron(III) site of met-azidohaemerythrin. In particular, the $O^{2-} \rightarrow Fe$ c.t. transitions appearing at 326 and 680 nm in the spectrum of the protein are very closely mimicked by those at 323 and 660 nm in that of **2**. Despite differences in the number of carboxylato bridges this similarity is perhaps not surprising given that both systems contain $N_3(O_2CR)_2$ donor sets about each of the iron(III) centres and that the μ-oxo-diiron(III) cores are of comparable dimensions. The spectrum of ribonucleotide reductase B2 is somewhat less similar to that of **2**, despite the presence of similar doubly bridged cores in both systems. This is attributed to the fact that the co-ordination environment for the active site of the protein is dominated by oxygen ligating groups, whilst that of **2**, despite the presence of terminal acetate groups, is rich in amine donors.

Interestingly, the bands observed for complex **2** are significantly blue shifted relative to those of the triply bridged cores capped by the ligands tacn (1,4,7-triazacyclononane) and its 1,4,7-trimethyl derivative which contain the same triamine ring as L. For the forbidden $O^{2-} \rightarrow Fe$ c.t. bands, which occur at 527 and 660 nm for **2** compared to *ca.* 550 and 740 nm for the triply bridged species, this effect may be ascribed to the somewhat larger Fe–O–Fe angle observed for **2** (Table 3). The larger Fe–O–Fe angle enhances π bonding between the iron(III) centres and the oxo bridge, decreasing both the Lewis acidity of the centres and the basicity of the oxo group, and thus increasing the splitting between the oxo donor and iron(III) acceptor orbitals.[27a,e]

In conclusion, we have synthesized both mono- and dinuclear iron(III) complexes of the tetradentate ligand L. The dinuclear complex, **2**, represents an addition to the series of reported doubly bridged μ-oxo-μ-carboxylato-diiron(III) complexes, which are relatively rare compared to their triply bridged counterparts. Its spectroscopic and magnetic properties are characterisitic of the oxo-bridged core, and are in accordance with those of the doubly bridged species reported by Que and co-workers.[11] A number of the features of the μ-oxo-diiron(III) sites present in the metalloproteins ribonucleotide reductase B2 and met-azidohaemerythrin are successfully mimicked by **2**. An interesing feature in the structure of **2** is the bridging of the sodium ion between the pendant carboxylate oxygen atoms co-ordinated to the iron(III) centres. Given the similarities of the structural and physicochemical features of **2** to those of other related μ-oxo-diiron(III) complexes, this bridging interaction appears to have little influence on the overall geometry or properties of the complex, and its existence is probably simply a consequence of the oxygen atoms being predisposed to such an interaction. It would be interesting to examine the possiblity of binding other cations and the effects that such binding might have on the intrinsic properties of the μ-oxo-diiron(III) core.

Experimental

Reagent or analytical grade materials were obtained from commercial suppliers and used without further purification. 1,4,7-Triazacyclononane-*N*-acetate dihydrochloride (L·2HCl) was prepared from 1,4,7-triazacyclononane according to the method of Studer and Kaden[13] and also by the method of Wieghardt and co-workers[14] which was reported during the course of this work. Proton and ^{13}C NMR spectroscopic data were in excellent agreement with those reported by these workers.

Infrared spectra were measured on a Perkin-Elmer 1600 Series FT-IR spectrophotometer as KBr pellets, electronic spectra on a Cary 3 spectrophotometer. Electron microprobe analyses

were made with a JEOL JSM-1 scanning electron microscope through an NEC X-ray detector and pulse-processing system connected to a Packard multichannel analyser. Microanalyses were performed by Chemical and Micro-Analytical Services (CMAS), Melbourne, Australia. Variable-temperature magnetic susceptibility measurements on powdered samples were carried out on a Quantum Design MPMS SQUID magnetometer using an applied field of 1 T. Mössbauer spectra were measured using a standard electromechanical transducer operating in a symmetrical constant-acceleration mode. A conventional nitrogen-bath cryostat was employed for temperature control with the samples maintained in exchange gas. Data were collected with an LSI-based 1000 multichannel analyser. Velocity calibration was with respect to iron foil. Spectra were fitted with a Lorentzian lineshape.

CAUTION: Although no problems were encountered in this work, perchlorate salts of transition metal complexes are potentially explosive and should thus be prepared in small quantities and handled with care.

Preparation of complexes

[$FeCl_2L$] 1. A solution of L·2HCl (0.500 g, 1.92 mmol) in distilled water (10 cm^3) was adjusted to pH 7 with sodium hydroxide solution (2 mol dm^{-3}) and $FeCl_3·6H_2O$ (0.519 g, 1.92 mmol) added to produce a dark yellow solution (pH ≈ 2). After standing overnight, orange-yellow crystals formed, which were filtered off, washed with ethanol and dried under vacuum (0.379 g, 63%) (Found: C, 30.6; H, 5.2; N, 13.6. $C_8H_{16}Cl_2FeN_3O_2$ requires C, 30.7; H, 5.2; N, 13.4%); ν_{max}/cm^{-1} 3272s, 3204s, 1660vs and 1325s (KBr). Electron microprobe: Fe and Cl uniformly present.

[LFe(μ-O)(μ-O_2CMe)FeL]ClO_4·$NaClO_4$·$2H_2O$ 2. A solution of sodium acetate (0.500 g, 6.09 mmol) and sodium perchlorate (0.500 g, 4.08 mmol) dissolved in distilled water (10 cm^3) was added to a solution of complex **1** (0.300 g, 0.958 mmol) in distilled water (5 cm^3) producing a brownish green solution. After standing for 1 week dark green crystals had formed, which were filtered off, washed with ethanol and dried under vacuum (0.211 g, 54%) (Found: C, 27.2; H, 5.1; N, 11.0. $C_{18}H_{39}Cl_2Fe_2N_6NaO_{17}$ requires C, 26.5; H, 4.8; N, 10.3%); ν_{max}/cm^{-1} 3622s, 3312s, 1636vs, 1543s, 1450s, 1347s, 1308s, 1092vs and 625s (KBr). Electron microprobe: Fe, Na and Cl uniformly present.

Crystallography

Intensity data for a yellow needle crystal of complex **1** (dimensions 0.32 × 0.08 × 0.06 mm) and a dark green prismatic crystal of **2** (0.48 × 0.28 × 0.20 mm) were measured at 296 K on a Rigaku AFC6R diffractometer equipped with graphite-monochromated Cu-Kα radiation for **1** and a Rigaku AFC6S diffractometer with graphite-monochromated Mo-Kα radiation for **2**. Cell constants were obtained from a least-squares refinement using the setting angles of 25 carefully centred reflections in the range $91.95 < 2\theta < 98.45°$ for **1** and $27.80 < 2\theta < 31.52°$ for **2**. For both complexes the data were collected using the ω–2θ scan technique. The intensities of three representative reflections were measured after every 150. No decay correction was necessary. An empirical absorption correction based on azimuthal scans of several reflections was applied in each case. The data were corrected for Lorentz-polarisation effects. Crystal parameters and details of the data collection and refinement for **1** and **2** are summarised in Table 5.

The structures were solved by direct methods (program SIR 92)[28] and expanded using standard Fourier routines in the TEXSAN software package.[29] Non-hydrogen atoms were refined with anisotropic thermal parameters. Hydrogen atoms were included in the models at their calculated positions (C–H 0.97 Å) but not refined. Full-matrix least-squares refinement minimised the function $\Sigma w(|F_o| - |F_c|)^2$ in each case and converged to the unweighted and weighted R factors given in Table 5. Molecular plots were drawn using the ORTEP program[16] with thermal ellipsoids at the 40% probability level.

Atomic coordinates, thermal parameters, and bond lengths and angles have been deposited at the Cambridge Crystallographic Data Centre (CCDC). See Instructions for Authors, *J. Chem. Soc., Dalton Trans.*, 1997, Issue 1. Any request to the CCDC for this material should quote the full literature citation and the reference number 186/361.

Acknowledgements

This work was supported by separate grants (to L. S. and K. S. M.) from the Australian Research Council. B. G. is the recipient of an Australian Postgraduate Award.

References

1 (*a*) R. G. Wilkins, *Chem. Soc. Rev.*, 1992, 171; (*b*) J. B. Vincent, G. L. Olivier-Lilley and B. A. Averill, *Chem. Rev.*, 1990, **90**, 1447; (*c*) L. Que, jun. and R. C. Scarrow, *ACS Symp. Ser.*, 1988, **372**, 152; (*d*) L. Que, jun. and A. E. True, *Prog. Inorg. Chem.*, 1990, **38**, 97; (*e*) S. J. Lippard, *Angew. Chem., Int. Ed. Engl.*, 1988, **27**, 344; (*f*) A. L. Feig and S. J. Lippard, *Chem. Rev.*, 1994, **94**, 759; (*g*) D. M. Kurtz, jun., *Chem. Rev.*, 1990, **90**, 585.
2 (*a*) R. G. Wilkins and P. C. Harrington, *Adv. Inorg. Biochem.*, 1983, **5**, 51; (*b*) K. Garbett, D. W. Darnall, I. M. Klotz and R. J. P. Williams, *Arch. Biochem. Biophys.*, 1969, **135**, 419; (*c*) P. C. Wilkins and R. G. Wilkins, *Coord. Chem. Rev.*, 1987, **79**, 195.
3 (*a*) B.-M. Sjöberg and A. Gräslund, *Adv. Inorg. Biochem.*, 1983, **5**, 87; (*b*) M. Lammers and H. Follmann, *Struct. Bonding (Berlin)*, 1983, **54**, 27; (*c*) P. Reichard and A. Ehrenberg, *Science*, 1983, **221**, 514; (*d*) L. Petersson, A. Gräslund, A. Ehrenberg, B.-M. Sjöberg and P. Reichard, *J. Biol. Chem.*, 1980, **255**, 6706.
4 M. P. Woodland, D. S. Patil, R. Cammack and H. Dalton, *Biochim. Biophys. Acta*, 1986, **873**, 237; A. Ericson, B. Hedman, K. O. Hodgson, J. Green, H. Dalton, J. G. Bentsen, R. Beer and S. J. Lippard, *J. Am. Chem. Soc.*, 1988, **110**, 2330; B. G. Fox, K. K. Sererus, E. Münck and J. D. Lipscomb, *J. Biol. Chem.*, 1988, **263**, 10553.
5 B. C. Antanaitis and P. Aisen, *Adv. Inorg. Biochem.*, 1983, **5**, 111.
6 (*a*) K. Wieghardt, J. Pohl and W. Gebert, *Angew. Chem., Int. Ed. Engl.*, 1983, **22**, 727; (*b*) A. Spool, I. D. Williams and S. J. Lippard, *Inorg. Chem.*, 1985, **24**, 2156.
7 (*a*) K. Wieghardt, K. Pohl and D. Ventur, *Angew. Chem., Int. Ed. Engl.*, 1985, **24**, 392; (*b*) J. R. Hartman, R. I. Rardin, P. Chaudhuri, K. Pohl, K. Wieghardt, B. Nuber, J. Weiss, G. C. Papaefthymiou, R. B. Frankel and S. J. Lippard, *J. Am. Chem. Soc.*, 1987, **109**, 7387.
8 W. H. Armstrong and S. J. Lippard, *J. Am. Chem. Soc.*, 1983, **105**, 4837.
9 J. W. Dawson, H. B. Gray, H. E. Hoenig, G. R. Rossman, J. M. Schredder and R. H. Wang, *Biochemistry*, 1972, **11**, 461.
10 R. E. Stenkamp, L. C. Sieker and L. H. Jensen, *Acta Crystallogr., Sect. B*, 1983, **39**, 697.
11 (*a*) S. Yan, D. D. Cox, L. L. Pearce, C. Juarez-Garcia, L. Que, jun., J. H. Zhang and C. J. O'Connor, *Inorg. Chem.*, 1989, **28**, 2507; (*b*) R. E. Norman, S. Yan, L. Que, jun., G. Backes, J. Ling, J. Sanders-Loehr, J. H. Zhang and C. J. O'Connor, *J. Am. Chem. Soc.*, 1990, **112**, 1554; (*c*) S. Mènage and L. Que, jun., *New J. Chem.*, 1991, **15**, 431.
12 P. Nordlund, B.-M. Sjöberg and J. Eklund, *Nature (London)*, 1990, **345**, 593.
13 M. Studer and T. A. Kaden, *Helv. Chim. Acta*, 1986, **69**, 2081.
14 D. Schulz, T. Weyhermüller, K. Wieghardt and B. Nuber, *Inorg. Chim. Acta*, 1995, **240**, 217.
15 G. B. Deacon and F. Huber, *Inorg. Chim. Acta*, 1985, **104**, 41.
16 C. K. Johnson, ORTEP II, ORNL Report 5136, Oak Ridge National Laboratory, Oak Ridge, TN, 1976.
17 (*a*) R. C. Scarrow, M. J. Maroney, S. M. Palmer, L. Que, jun., A. L. Roe, S. P. Salowe and J. Stubbe, *J. Am. Chem. Soc.*, 1987, **109**, 7857; (*b*) G. Bunker, L. Petersson, B.-M. Sjöberg, M. Sahlin, M. Chance, B. Chance and A. Ehrenberg, *Biochemistry*, 1987, **26**, 4708.
18 P. E. Clark and J. Webb, *Biochemistry*, 1981, **20**, 4628.
19 C. L. Atkins, L. Thelander, P. Reichard and G. Lang, *J. Biol. Chem.*, 1973, **248**, 7464.

20 K. S. Murray, *Coord. Chem. Rev.*, 1974, **12**. 1.
21 D. E. Fenton, in *Comprehensive Coordination Chemistry*, eds. G. Wilkinson, R. D. Gillard and J. A. McCleverty, Pergamon, Oxford, 1987, vol. 3, pp. 1–80.
22 K. Wieghardt, U. Bossek, P. Chaudhuri, W. Herrmann, B. C. Menke and J. Weiss, *Inorg. Chem*., 1982, **21**, 4308.
23 G. Fachinetti, C. Floriani, P. F. Zanazzi and A. R. Zanzari, *Inorg, Chem.*, 1979, **18**, 3469.
24 D. Schulz, T. Weyhermüller, K. Wieghardt, C. Butzlaff and A. X. Trautwein, *Inorg. Chim. Acta*, 1996, **246**, 387.
25 S. M. Gorun and S. J. Lippard, *Inorg. Chem.*, 1991, **30**, 1625.
26 T. C. Gibb and N. N. Greenwood, *Mössbauer Spectroscopy*, Chapman and Hall, London, 1971.
27 (*a*) R. C. Reem, J. M. McCormick, D. E. Richardson, F. J. Devlin, P. J. Stephens, R. L. Musselman and E. I. Solomon, *J. Am. Chem. Soc.*, 1989, **111**, 4688; (*b*) K. D. Butcher, M. J. Gebhard and E. I. Solomon, *Inorg. Chem*., 1990, **29**, 2067; (*c*) J. Sanders-Loehr, W. D. Wheeler, A. K. Shiemke, B. A. Averill and T. M. Loehr, *J. Am. Chem. Soc.*, 1989, **111**, 8084; (*d*) R. S. Czernuszewicz, J. E. Sheats and T. G. Spiro, *Inorg. Chem*., 1987, **26**, 2063; (*e*) R. E. Norman, R. C. Holz, S. Ménage, C. J. O'Connor, J. H. Zhang and L. Que, jun., *Inorg. Chem*., 1990, **29**, 4629.
28 A. Altomare, M. Cascarano, C. Giacovazza and A. Guagliardi, *J. Appl. Crystallogr.*, 1993, **26**, 4629.
29 TEXSAN, Crystal Structure Analysis Package, Molecular Structure Corporation, Houston, TX, 1985 and 1992.

Received 27*th September* 1996; *Paper* 6/06651H